HHS Public Access

Author manuscript

Macromol Biosci. Author manuscript; available in PMC 2023 January 26.

Published in final edited form as:

Macromol Biosci. 2022 August ; 22(8): e2200103. doi:10.1002/mabi.202200103.

3D-Printed Electroactive Hydrogel Architectures with Sub-100 μm Resolution Promote Myoblast Viability

Rebecca L. Keate,
Department of Biomedical Engineering, Northwestern University, Evanston, IL 60208, USA

Center for Advanced Regenerative Engineering, Northwestern University, Evanston, IL 60208, USA

Simpson Querrey Institute, Northwestern University, Chicago, IL 60611, USA

Joshua Tropp,
Department of Biomedical Engineering, Northwestern University, Evanston, IL 60208, USA

Center for Advanced Regenerative Engineering, Northwestern University, Evanston, IL 60208, USA

Simpson Querrey Institute, Northwestern University, Chicago, IL 60611, USA

Caralyn P. Collins,
Mechanical Engineering Department, Northwestern University, Evanston, IL 60208, USA

Henry Oliver T. Ware,
Mechanical Engineering Department, Northwestern University, Evanston, IL 60208, USA

Anthony J. Petty II,
Department of Biomedical Engineering, Northwestern University, Evanston, IL 60208, USA

Center for Advanced Regenerative Engineering, Northwestern University, Evanston, IL 60208, USA

Simpson Querrey Institute, Northwestern University, Chicago, IL 60611, USA

Guillermo A. Ameer,
Department of Biomedical Engineering, Northwestern University, Evanston, IL 60208, USA

Center for Advanced Regenerative Engineering, Northwestern University, Evanston, IL 60208, USA

Cheng Sun,
Mechanical Engineering Department, Northwestern University, Evanston, IL 60208, USA

jrivnay@northwestern.edu .

Supporting Information

Supporting Information is available from the Wiley Online Library or from the author.

Conflict of Interest

The authors declare no conflict of interest.

Jonathan Rivnay
Department of Biomedical Engineering, Northwestern University, Evanston, IL 60208, USA

Center for Advanced Regenerative Engineering, Northwestern University, Evanston, IL 60208, USA

Simpson Querrey Institute, Northwestern University, Chicago, IL 60611, USA

Abstract

3D-printed hydrogel scaffolds functionalized with conductive polymers have demonstrated significant potential in regenerative applications for their structural tunability, physiochemical compatibility, and electroactivity. Controllably generating conductive hydrogels with fine features, however, has proven challenging. Here, micro-continuous liquid interface production (μCLIP) method is utilized to 3D print poly(2-hydroxyethyl methacrylate) (pHEMA) hydrogels. With a unique in-situ polymerization approach, a sulfonated monomer is first incorporated into the hydrogel matrix and subsequently polymerized into a conjugated polyelectrolyte, poly(4-(2,3-dihydro-thieno[3,4-*b*][1,4]dioxin-2-ylmethoxy)-butane-1 sulfonic acid sodium salt (PEDOT-S). Rod structures are fabricated at different crosslinking levels to investigate PEDOT-S incorporation and its effect on bulk hydrogel electronic and mechanical properties. After demonstrating that PEDOT-S does not significantly compromise the structures of the bulk material, pHEMA scaffolds are fabricated via μCLIP with features smaller than 100 μm. Scaffold characterization confirms PEDOT-S incorporation bolstered conductivity while lowering overall modulus. Finally, C2C12 myoblasts are seeded on PEDOT-pHEMA structures to verify cytocompatibility and the potential of this material in future regenerative applications. PEDOT-pHEMA scaffolds promote increased cell viability relative to their non-conductive counterparts and differentially influence cell organization. Taken together, this study presents a promising new approach for fabricating complex conductive hydrogel structures for regenerative applications.

Graphical Abstract

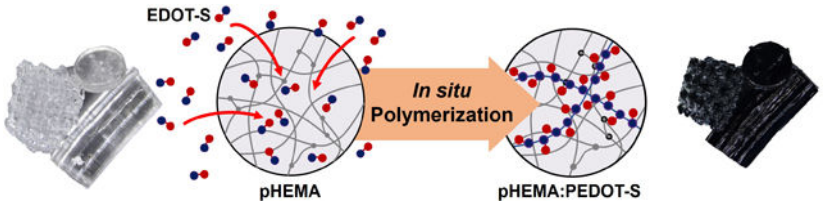

Keywords

3D-printing; conductive hydrogels; conductive polymers

1. Introduction

Considering the complexity of physiological systems targeted with tissue engineering developments, any novel biomaterial aiming to facilitate repair needs to satisfy a variety of criteria. These requirements include, but are not limited to, mimicking the structural complexity of tissue from the micro-to macro-scale, physiologically integrating with the

tissue environment, and promoting bioactive processes which accelerate regeneration.[1] Three dimensional (3D) printed hydrogels have rapidly emerged as a powerful tool to satisfy these fundamental requirements owing to their customizable structure,[2] high-water content,[3,4] and ability to specifically direct cell fate via incorporation of growth factors or other physiologically potent molecules.[5]

Electroactive components, such as conductive polymers,[3,6–8] metallic nanoparticles,[9] or various graphene derivatives[10,11] are commonly incorporated into hydrogel systems to potentiate physiological outcomes. While several studies have noted that such electroactive fillers have a high capacity to drive cellular outcomes, the mechanisms by which electronic elements yield physiological benefits, such as cell proliferation and differentiation, remain unclear. Of these various electroactive materials, conductive polymers are among the most potent in influencing cell functionality, with or without external electrical stimulus, due to their mixed ionic/electronic conduction mechanisms,[12] synthetic tailorability,[13] biocompatibility,[14] and mechanical properties[15] all of which can facilitate biomaterial integration.[16] Despite these benefits, the limited solubility and hydrophobicity of conductive polymers often complicate their incorporation into hydrophilic biomaterials such as hydrogels. Bulk electroactivity of conductive polymer-functionalized hydrogels relies on the formation of a homogeneous interpenetrating network, yet functionalization with conductive polymers commonly causes aggregation of the conductive polymer and phase separation from the hydrogel, thus hindering bulk material conductivity and deleteriously effecting bulk mechanical properties.[3,17]

One of the most significant challenges in the current conductive hydrogel landscape is achieving and maintaining structural control of fine (<200 μm) features, an important requirement in soft bioelectronics and robotics, where the function of a device is highly dependent on its morphological stability.[7,18] Conductive polymer incorporation in 3D printed hydrogels generally relies on in-situ polymerization rather than a direct polymer blending approach, as conjugated monomers can more easily diffuse throughout the hydrogel matrix.[6] Such systems, however, are limited to large features (500 μm–1000 μm) and are often too brittle to function reliably.[18,19] A reproducible method to generate conductive features at fine (<200 μm) size scales would not only be useful for mechanistic investigations but would also enable the development of more effective advanced bioelectronic systems such as neural probes or other sensing technologies.

Common 3D printing approaches, such as stereolithography, have also limited the architectural control of conductive polymer hydrogels. These traditional 3D printing techniques are accompanied by a tradeoff between feature resolution and printing duration, and as a result, fabrication of micron-scale structures requires impractically long print time. The advent of micro-continuous liquid interface production (μCLIP) in stereolithography facilitates the generation of complex hydrogels in a significantly more time-efficient and mechanically consistent manner (Figure 1a).[20,21] Poly(2-hydroxyethyl methacrylate) (pHEMA), a polymer prevalently used in biomaterials along with the crosslinker ethylene glycol dimethacrylate (EGDMA), is compatible with the μCLIP technique, and can be leveraged to achieve more precise and reliable control over hydrogel architecture.[22] While pHEMA hydrogels demonstrate particularly high structural fidelity in addition to favorable

biocompatibility,[23] they have yet to be printed into complex structures, such as scaffolds, with features smaller than 100 μm.

Here, we adopt a two-step approach to incorporate conductive materials within pHEMA hydrogels (Figure 1c,d). We demonstrate that by utilizing an in situ polymerization strategy, conductive polymers can reproducibly interpenetrate finer hydrogel structures for enhanced bioelectronic applications. The approach here leverages sulfonated 3,4-ethylenedioxy thiophene (EDOT)-derivative, EDOT-S, which exhibits extremely high aqueous solubility compared to traditionally utilized monomers such as aniline, pyrrole, or EDOT, and therefore, enables simple loading of monomers (to be polymerized into a conductive polymer) into prefabricated hydrogel structures, without using any organic solvents that could deleteriously affect biomaterials or their intended application. Printing conditions were optimized by adjusting the loading of EGDMA within the resin to maximize the functionalization efficacy of sub-100 μm features, demonstrating that bulk material properties can be altered with EGDMA manipulation alone. Finally, we demonstrate that these composites have favorable cytocompatibility by examining the morphology and viability of C2C12 mouse myoblasts on PEDOT-S functionalized pHEMA (PEDOT-pHEMA). Overall, this study outlines a novel approach that leverages a conjugated polymer incorporation strategy, while optimizing hydrogel crosslinking levels, to generate conductive structures with size scales previously unrealized that bolster cell viability and differentially influences cellular organization compared to its non-conductive counterpart.

2. Results and Discussion

2.1. Crosslinking Differentially Influences Electrical Properties and Mechanical Properties

Systematic manipulation of EGDMA loading was performed to determine how the pHEMA crosslinking influenced the material characteristics of the functionalized composites. Rod form factors were adopted as a model system with simple macroscale geometries that allowed us to collect reliable mechanical and electronic datasets, thus informing the design of more complex structures. The cylindrical geometry also facilitates translatability toward a broad range of applications such as mechanistic investigations with micropillars or clinical applications such as nerve graft conduits.[25]

We analyzed cylindrical hydrogel rods to evaluate the relationship between EGDMA crosslinking and bulk PEDOT-pHEMA properties. Rods were cut along the sagittal plane to verify that a color change attributable to PEDOT-S presence was apparent within the rods (Figure S4a, Supporting Information). Energy-dispersive X-ray spectroscopy (EDS) was performed on PEDOT-pHEMA rod cross-sections to verify that the polymer penetrated throughout the bulk of the rod (Figure S4b,c, Supporting Information). We observed that sulfur was present throughout the entire rod cross-section, and not localized at the outer surface, verifying that PEDOT-S penetrated the bulk of the pHEMA.

Electrochemical impedance spectroscopy (EIS) was used to extract the electrical properties of the pHEMA rods, revealing an inverse relationship between EGDMA crosslinking and the rod conductivity for both the PEDOT-pHEMA and the pHEMA cases (Figure 2a). A custom apparatus was designed to measure electrical properties, so the rods could be consistently

secured between two ITO glass slides during and between measurements (Figure S5c, Supporting Information). The use of nylon screws to secure the custom-designed ITO slide holders led to a highly stable and reproducible unit that ensured spacing was consistent during measurements (Figure S5, Supporting Information). Measured conductivities were 0.161 ± 0.040, 0.072 ± 0.027, 0.013 ± 0.009, and 0.007 ± 0.001 mS cm^{-1} for 0.5%, 0.75%, 1%, and 3% EGDMA pHEMA rods respectively. After functionalization, these conductivities increased to 2.561 ± 0.709, 1.788 ± 0.055, 0.972 ± 0.275, and 0.497 ± 0.095 mS cm^{-1}. In all cases, increases in conductivity were significant. We attribute this trend to higher loading levels of PEDOT-S, by virtue of monomer diffusivity, which is facilitated at lower crosslinking levels. Previous studies that utilize similar functionalization protocols to the one described here, where the monomer is loaded into the hydrogel structure prior to polymerization, report conductivity values comparable to those measured in this study.[26]

After evaluating the influence of crosslinking on the electrical properties of the rods, the elastic modulus of the rods was evaluated via compression testing. During compression, the rods demonstrated stress-strain curves that were largely linear, with each rod demonstrating maximum compression between 10% and 12% strain. As expected, a significant increase in modulus was observed with increased crosslinking of the hydrogel matrix, with pHEMA hydrogels containing 3% EGDMA demonstrating higher moduli than those containing 0.5%, 0.75%, or 1% EGDMA (Figure 2b). Comparing the control pHEMA hydrogels to those functionalized with PEDOT-S, no significant differences in moduli were observed, regardless of EGDMA loading level.

This result is unique to the system presented here, as similar hydrogels demonstrate increased stiffness upon the incorporation of conductive polymers.[25] We attribute the comparable mechanical properties of pHEMA and PEDOT-pHEMA to the use of a formally water-soluble and hygroscopic conjugated polymer rather than water-dispersible or insoluble counterparts which typically employ un-modified EDOT monomers.[27]

We further investigated the relationship between hydrogel crosslinking and PEDOT-S incorporation using thin disc structures, which allowed us to perform UV–vis spectroscopic analysis to estimate PEDOT-S content. Discs with 0.5% EGDMA loading were not evaluated here because the structures were too soft to be reliably printed and handled in such thin free-standing structures. In 500 μm thick discs, 0.75% EGDMA loading showed the highest PEDOT-S content whereas discs with 3% EGDMA loading demonstrated the lowest levels of PEDOT-S (Figure S3c, Supporting Information). The results of the electrical and mechanical testing with rods and the spectroscopic analysis of discs align with our hypothesis that reduced hydrogel crosslinking promotes higher levels of monomer loading via diffusion during incubation, increasing overall PEDOT-S incorporation and thus conductivity (Figure 2d). It remains unclear whether the slight but consistent differences in PEDOT-S loading observed in the thin discs are sufficient to account for the two- to three-fold differences observed in rod conductivity or modulus, or whether more complex morphological factors are at play. This phenomenon is a subject of further investigation. While these investigations utilized homogenous prints, future studies may be aimed at generating bulk structures with spatially variable crosslinking, which may improve there generative potential of complex biological systems.[28]

2.2. Fabrication of Electroactive Scaffolds with Features Sizes less than 100 μm

Prior to functionalization, we systematically evaluated the dimensions of the features throughout the printed scaffold to verify we had structures smaller than 100 μm. The smallest structures of the scaffolds were printed as inner scaffold struts. To ensure the whole unit was mechanically robust, larger supporting hexagonal units were included along the scaffold perimeter. We accomplished the feature size analysis by evaluating SEM images of three different scaffolds and measuring the features on the structure surface (Figure S8a, Supporting Information). Analyzing the distribution of feature sizes throughout the scaffolds showed the average feature size of those intended to be 120 μm was 114.7 ± 22.2 μm, and for the intended 100 μm features, the average size was 99.8 ± 19.3 μm (Figure S8b, Supporting Information). This analysis further verified that the printing protocol adopted here is sufficient for establishing hydrogel feature sizes less than 100 μm. Following functionalization, a notable color change was observed throughout the scaffold, including the smaller features, verifying the successful incorporation of PEDOT-S. This further supported the previous evidence that the protocol demonstrated here was effective for incorporating conductive polymers into the hydrogel matrix.

Considering the small feature sizes that were achieved with scaffold fabrication, we sought to understand whether the relationship between hydrogel crosslinking and PEDOT-S incorporation remained consistent throughout a range of feature sizes. We thus aimed to identify an ideal crosslinking condition for fine scaffold features by measuring PEDOT-S loading in thin pHEMA discs (Figure S3, Supporting Information). One hundred twenty-five micrometer thick discs were printed and evaluated through UV–vis, revealing the highest level of PEDOT-S incorporation with 1% EGDMA loading. Based on these results, we pursued the 1% crosslinking level to maximize PEDOT-S incorporation in the smallest features of the scaffolds. Taken together, the resin with 1% EGDMA crosslinking loading was utilized for the fabrication of more complex structures comprising small (≈100 μm) features. With design parameters informed by disc and rod characterizations, we pursued a scaffold structure to demonstrate (1) that the functionalization method lends itself towards complex structures with intricate features and (2) these structures have significant potential to be leveraged in regenerative applications.

2.3. PEDOT Incorporation Modifies Scaffold Electroactivity and Modulus

Scaffolds were fabricated as a proof-of-concept structure containing fine features to demonstrate that complex PEDOT-pHEMA architectures could be constructed with high stability and fidelity (Figure 3a). Additionally, the scaffold structure is more favorable for demonstrating the relevance of these materials in biological experiments such as mechanistic in vitro cell culture explorations.[29] Using the same protocol as was adopted with the printed rods, the electrical properties of the scaffolds were measured to ensure that PEDOT functionalization of a bulk structure with fine features still led to decreased impedance. EIS data were fitted to an RC circuit, where the fitted *R*-value was extracted and reported (Figure 3b). The average impedance for the control scaffold was 150.5 ± 59.7 kΩ, whereas the impedance for the PEDOT-pHEMA scaffold was significantly lower at 28.2 ± 9.8 kΩ. This analysis verified that PEDOT-S functionalization of the pHEMA scaffolds, with features less than 100 μm, yielded structures with bulk conductivity greater than that of the control.

Compression testing on pHEMA and PEDOT-pHEMA was also performed as previously described for the rods. Although no significant difference was observed between pHEMA and PEDOT-pHEMA rods, mechanical testing of the scaffolds revealed that the bulk structure was significantly softer with the addition of conductive polymer compared to the pHEMA control structure (Figure 3c). This result further suggests that the use of a conjugated polyelectrolyte, particularly considering the hydrophilic nature of PEDOT-S, may allow for increased diffusion of water into the structure (Figure S10, Supporting Information), leading to an electroactive structure with a lower modulus than the original hydrogel.

2.4. PEDOT-pHEMA Bolsters Cell Viability, Promotes Favorable Void Space Cytoskeleton Arrangement

To verify that the composites were not significantly cytotoxic, we seeded C2C12 myoblasts on scaffolds and assessed cell health. C2C12 cells serve as a highly relevant model system as they have been utilized to demonstrate the benefits of conductive substrates for myoblast maturation and muscle regeneration.[30,31]

The cell viability results demonstrated that at all three time points assessed (1–3 days), PEDOT-pHEMA scaffolds promoted greater cell health than the pHEMA scaffolds alone (Figure 4a). Live/dead staining was also performed to qualitatively examine the distribution of live and dead cells on the scaffolds after 24 h. We observed considerable background noise from the propidium iodide (red “dead” stain in Live/Dead assay) on both the pHEMA and PEDOT-pHEMA scaffolds. Although this complicates our ability to distinguish isolated dead cells, we still observed that cells seeded on the scaffolds were alive and adherent to the material in both cases (Figure 4b,c).

To qualitatively identify whether PEDOT-S led to differences in cytoskeleton arrangement, F-actin of the cell cytoskeleton was stained after five days in growth media. Cytoskeleton morphology is highly relevant for myoblasts, considering cytoskeletal order is a key parameter of differentiation and myotube formation.[10,30,32] We observed that cells seeded on the PEDOT-pHEMA scaffolds preferentially formed organized multicellular structures in the open porous space of the scaffold, whereas on the pHEMA control scaffolds, cells remained adhered to the scaffold itself. In instances where cells were observed in open space on the pHEMA scaffold, the cells appeared to be less organized compared to the open space cellular structures observed on the PEDOT-pHEMA scaffolds (Figure 4d,e). This result was unexpected, especially considering the dramatic increase in cell viability observed with cells seeded on the PEDOT-pHEMA scaffold. One point that may be beneficial for future investigation is the conductivity of the structure over the course of cell culture experiments. Due to the method of measuring impedance here, it was not feasible to measure changes in the structure’s overall conductivity throughout the course of cell culture experiments. The high ratio of EDOT:sulfonate groups, which is 1:1 in this functionalization regime, may generate hydrogels with a higher surface charge than other PEDOT-based conductive polymer hydrogels, but with electrical stimulation, the high ratio of monomer to dopant may be advantageous in driving cellular processes. Furthermore, the ability to tune cell assemblies in free space, rather than on the scaffold itself, is highly useful in various

biological applications requiring specific cell infiltration and will be the subject of future investigations.[33]

3. Conclusion

In this study, we demonstrated the successful fabrication of conductive pHEMA hydrogels with high fidelity features smaller than100 μm. While several studies have previously demonstrated the fabrication of conductive hydrogels with small features,[34] the reported methodology is unique in that electroactive hydrogels with more specific 3D structures can be fabricated to systematically target various bioelectronic applications. In part, these functionalization capabilities are attributable to the use of hydrophilic conjugated monomers. The sulfonate group of EDOTS facilitated more homogeneous incorporation of the conductive polymer networks within the hydrophilic pHEMA hydrogels.

Designing conductive hydrogels has previously presented several challenges, particularly in terms of maintaining structural stability with features less than 200 μm in size. We began characterization of this functionalization regime with pHEMA rods to evaluate whether PEDOT incorporation led to significant differences in material characteristics. We found an inverse relationship between EGDMA crosslinking and conductivity, yet PEDOT-S incorporation did not yield any significant differences in mechanical properties. The relationship between conductivity and EGDMA loading is attributed to crosslinking influencing monomer diffusion into the hydrogel structures. This result was corroborated by spectroscopic analysis of 500 μm thick discs, which demonstrated an inverse relationship between PEDOT-S loading and crosslinking. The lack of a significant increase in hydrogel modulus following conductive polymer incorporation is unique to the system described here.

Finally, we fabricated PEDOT-pHEMA scaffolds with stable features less than 100 μm using 1% EGDMA loading and demonstrated the promise of these scaffolds to drive cellular outcomes in future applications with C2C12 myoblasts. Performing cell viability assays, we observed bolstered health in cells grown on the PEDOT-pHEMA scaffolds compared to those grown on pHEMA scaffolds alone. Differences in cell organization on the scaffolds were also observed, whereas on the PEDOT-pHEMA scaffolds, cells were inclined to grow into the open space of the scaffolds rather than adhering strictly to the material. These differences in cellular outcomes can be attributed to the conductive polymer functionalization of the pHEMA scaffold. Future efforts will focus on exploring the interactions between these materials and cellular processes to better understand how the composites may be leveraged in regenerative engineering. Later studies may also explore the use of natural polymers such as alginate or agarose to fabricate the scaffolds, rather than pHEMA. Natural materials are more likely to enhance cell adhesion, which may further bolster the regenerative benefits of the PEDOT-functionalized hydrogels.[35]

4. Experimental Section

EDOT-S Synthesis:

All manipulations of air and/or moisture-sensitive compounds were performed under an inert atmosphere using standard glove box and Schlenk techniques. Reagents for monomer

synthesis were purchased from Sigma-Aldrich and used without further purification. 4-(2,3Dihydrothieno[3,4-*b*][1,4]dioxin-2-yl-methoxy)-1-butanesulfonic acid and sodium salt (EDOT-S) were prepared according to previously reported procedures.[24]

3D Printing pHEMA:

A home-made μCLIP printer was used to print all structures utilized throughout the study. Conditions used for printer setup and operation followed previously reported procedures.[20] Focal plane pixel resolution was set at 7.1 μm × 7.1 μm, and 5 μm layer thickness as previously described.[19] Hydrogel resin consisted of (hydroxyethyl)methacrylate (HEMA) as a monomer, Irgacure 819 as a photoinitiator, and varying levels of EGDMA as a crosslinker (Table S1, Supporting Information). After combining the HEMA, EGDMA, and Irgacure 819, the ink was sonicated for ≈1 h until homogeneous.

Using the μCLIP printer, disc, rod, and scaffold form factors were printed (Figure 1b). pHEMA discs were printed at a constant diameter of 2 mm and varying thicknesses of 125 μm, 500 μm, and 1 mm to analyze the relationship between PEDOT-S incorporation and EGDMA crosslinking. Discs of 500 μm and 1 mm in thickness were printed with a continuous stage speed of 2.40 μm s^{-1} (a per individual projected image exposure time of 2.08 s), while 125 μm thick discs required a stage speed of 1.74 μm s^{-1} (per image exposure time of 2.88 s) to withstand handling. 2 mm diameter rods were printed using a stage speed of 1.62 μm s^{-1} (per image exposure time of 3.08 s) to characterize the influence of crosslinking and PEDOT-S functionalization on the bulk hydrogel properties. After analysis of disc and rod structures, pHEMA scaffolds were fabricated. Scaffolds consisting of repeating 3D hexagonal unit cells were designed with the goal of developing stable structures with features smaller than 100 μm (Figure S8, Supporting Information). The larger features could be found around the perimeter of the scaffold, providing structural support, while the smallest features of the unit were within the structure's core. Scaffolds were printed with an optimized cure time of 3.08 s per fabrication layer, as was used for the rods. All prints used a constant UV power density of ≈4.02 m<Di>W cm^{-2} for the base layer cure and 3.16 mW cm^{-2} for the rest of the structure.

Material Functionalization:

After printing, the pHEMA structures were soaked in acetone for at least 24 h to ensure any remaining photoinitiator leached out of the scaffold. Prior to beginning functionalization, materials were rinsed in deionized (DI) water to wash acetone from the hydrogels. The pHEMA structures were then incubated in 400 mg mL^{-1} of EDOT-S for 4 h at 37 °C. After incubation in EDOT-S, a polymerization solution was prepared by adding ammonium persulfate and phytic acid to EDOT-S for a final concentration of 0.35 m. Structures were incubated in the polymerization solution overnight at 4 °C, rinsed, and kept in deionized (DI) water at room temperature for at least 24 h prior to analysis. For all experiments, control pHEMA structures were prepared by soaking in Dulbecco's Phosphate-Buffered Saline (DPBS) solution without EDOT-S. Similarly, all control structures were exposed to the polymerization solutions without EDOT-S.

Material Characterization:

pHEMA and PEDOT-pHEMA discs of varying thicknesses (1 mm, 500 μm, and 125 μm), as well as different crosslinking conditions (0.75 wt.%, 1 wt.%, and 3 wt.%), were characterized using UV–vis spectroscopy. Discs were mounted on the stage of a NanoDrop One (Thermo Scientific), and absorption spectra were collected. After collecting the spectra, the absorbances at 700 nm were averaged and compared.

Electrochemical Impedance Spectroscopy (EIS) was used to assess the electrical properties of the pHEMA rods and scaffolds. For PEDOT-pHEMA rods, the electrical properties were measured with varying crosslinking conditions (0.5 wt.%, 0.7 wt.%, 1 wt.%, and 3 wt.%) to elucidate the relationship between bulk electrical properties and EGDMA crosslinking. EIS was performed on scaffolds at 1 wt.% EGDMA crosslinking. A custom apparatus was designed to repeatedly mount rods and scaffolds for electrical testing (Figure 2a; Figure S5, Supporting Information). EIS was run at 31 frequencies between 0.1–1 × 10^6 Hz with a 10 mV RMS AC amplitude. The resulting data were fit to an equivalent RC circuit with a resistor and capacitor in series, excluding frequencies above 1000 Hz. The R and C values were extracted based on the circuit fits, and those numbers were averaged. Conductivity values were calculated based on the extracted resistance value. All rods were estimated to have a radius of 1 mm and were sliced into 4 mm long units with a razor.

Mechanical properties of scaffolds and rods were analyzed via compression testing. Compression tests were performed on a TA Instruments RSA G2 Dynamic Mechanical Analyzer (DMA) applying strain at a rate of 0.03 mm s^{-1} until the samples reached equilibrium. The modulus of the materials was then calculated from the slope of the linear portion of the stress-strain curve. A custom MATLAB program was written to systematically identify the linear region of the curve and perform a linear regression. The cross-sectional area of the scaffold at the contact interface was estimated to be 5.26 mm^2.

Scanning electron microscopy (SEM) and energy-dispersive X-ray spectroscopy (EDS) were both performed on a Hitachi SU8030 microscope. Before imaging, all specimens were coated with 15 nm of Au/Pd using a Denton III Desk Sputter Coater. EDS was performed to map the sulfur distribution of pHEMA and PEDOT-pHEMA rods that were lyophilized and cut transversely. AZtec software was used to collect the EDS maps of the rod cross-sections. SEM was performed on pHEMA scaffolds, and Quartz PCI software was then used to measure the size of each feature in the structure.

Cell Culture:

C2C12 cells were acquired from ATCC and cultured under standard culture conditions. Specifically, cells were maintained in an incubator at 37 °C with 5% CO_2. During expansion, cells were grown in low glucose DMEM supplemented with 10% Fetal Bovine Serum and 1% antibiotic/antimycotic.

Cells were seeded on scaffolds at a density of 5 × 10^4 cells cm^{-2}. Cells were seeded in four different quadrants of the scaffold, in four separate 2 μL drops. After the initial seeding, cells were placed in the incubator for ≈1 h to allow for attachment prior to adding media. Prior to the first cell viability measurement, scaffolds were placed in a new well to ensure

cell health measurements were not confounded by any cells remaining on the bottom of the well. After 24, 48, and 72 h in culture, cell viability was quantified using an alamarBlue cell viability assay (Thermo). The assay was conducted according to the manufacturer's protocol. Briefly, cell media was removed and replaced with cell media containing 10% by volume alamarBlue reagent. Scaffolds were then incubated in this media for 4 h. After the incubation period, the fluorescence of the media was measured at 560 nm emission and 590 nm excitation with a Cytation3 plate reader. Here, the average measured fluorescence was reported in Relative Fluorescence Units (RFU).

Live/dead staining (Thermo), shown in green and red respectively, was performed to qualitatively examine cell morphology and distribution on the scaffold of cells in culture for 24 h. After five days in culture, scaffolds were rinsed in DPBS three times and fixed in 4% paraformaldehyde for 15 min. Samples were then rinsed again three times with DPBS and immobilized with a blocking buffer containing 0.2% Triton-X and 5% bovine serum albumin (BSA). Cells were then soaked in phalloidin stain (green) to label cytoskeleton F-actin at a 1:200 dilution in blocking buffer for 1.5 h. Following phalloidin incubation, scaffolds were rinsed three times with DPBS, with the second rinse containing a 1:100 dilution of Hoechst stain to label the cell nuclei (blue). These images were taken as z-stacks with a Nikon A1 confocal microscope and Nikon Elements imaging software. The z-stacks were at least 100 μm in depth and were processed using ImageJ.

Supplementary Material

Refer to Web version on PubMed Central for supplementary material.

Acknowledgements

This work was primarily supported by Office for Naval Research (ONR) YIP (Grant No. N00014–20-12777). R.K. was supported in part by the National Institutes of Health Training Grant (Grant No. T32GM008449) through Northwestern University's Biotechnology Training Program. J.T. was primarily supported by an ONR YIP (Grant No. N00014–20-1–2777). C.C., H.T.O.W., G.A., and C.S. were supported in part by the National Institutes of Health (Grant No. R01HL141933 and R01DE030480). G.A. and A.P. acknowledge support from the Center for Advanced Regenerative Engineering at Northwestern University. This work made use of the EPIC facility of Northwestern University's NUANCE Center, which has received support from the SHyNE Resource (Grant No. NSF ECCS2025633), the IIN, and Northwestern's MRSEC program (Grant No. NSF DMR-1720139). This work made use of the DMA at the MatCI Facility supported by the MRSEC program of the National Science Foundation (Grant No. DMR-1720139) at the Materials Research Center of Northwestern University. Absorbance measurements were performed in the Analytical bioNanoTechnology Core Facility of the Simpson Querrey Institute at Northwestern University. ANTEC is currently supported by the Soft and Hybrid Nanotechnology Experimental (SHyNE) Resource (Grant No. NSF ECCS-2025633). Imaging work was performed at the Northwestern University Center for Advanced Microscopy generously supported by NCI CCSG P30 CA060553 awarded to the Robert H Lurie Comprehensive Cancer Center. This work made use of the IMSERC NMR facility at Northwestern University, which has received support from the Soft and Hybrid Nanotechnology Experimental (SHyNE) Resource (NSF ECCS-2025633), Int. Institute of Nanotechnology, and Northwestern University.

Data Availability Statement

The data that support the findings of this study are available from the corresponding author upon reasonable request.

References

[1]. a)Lin K, Zhang D, Macedo MH, Cui W, Sarmento B, Shen G, Adv. Funct. Mater. 2019, 29, 1804943;b)Thomson RC, Wake MC, Yaszemski MJ, Mikos AG, in Biopolymers II, Springer, Berlin 1995;c)Wang X, Rivera-Bolanos N, Jiang B, Ameer GA, Adv. Funct. Mater. 2019, 29, 1809009.

[2]. a)Heo DN, Castro NJ, Lee S-J, Noh H, Zhu W, Zhang LG, Nanoscale 2017, 9, 5055; [PubMed: 28211933] b)Jung JW, Lee J-S, Cho D-W, Sci. Rep. 2016, 6, 21685;c)Kong B, Sun L, Liu R, Chen Y, Shang Y, Tan H, Zhao Y, Sun L, Chem. Eng. J. 2022, 428, 131012.

[3]. Distler T, Boccaccini AR, Acta Biomater. 2020, 101, 1. [PubMed: 31476385]

[4]. Zhang XN, Wang YJ, Sun S, Hou L, Wu P, Wu ZL, Zheng Q, Macromolecules 2018, 51, 8136.

[5]. a)Burdick JA, Mason MN, Hinman AD, Thorne K, Anseth KS, J. Controlled Release 2002, 83, 53;b)Garrett Q, Laycock B, Garrett RW, Invest. Ophthalmol. Visual Sci. 2000, 41, 1687; [PubMed: 10845587] c)Wylie RG, Ahsan S, Aizawa Y, Maxwell KL, Morshead CM, Shoichet MS, Nat. Mater. 2011, 10, 799; [PubMed: 21874004] d)Yamamoto M, Ikada Y, Tabata Y, J. Biomater. Sci., Polym. Ed. 2001, 12, 77. [PubMed: 11334191]

[6]. Distler T, Polley C, Shi F, Schneidereit D, Ashton MD, Friedrich O, Kolb JF, Hardy JG, Detsch R, Seitz H, Boccaccini AR, Adv. Healthcare Mater. 2021, 10, 2001876.

[7]. Fantino E, Roppolo I, Zhang D, Xiao J, Chiappone A, Castellino M, Guo Q, Pirri CF, Yang J, Macromol. Mater. Eng. 2018, 303, 1700356.

[8]. Yuk H, Lu B, Lin S, Qu K, Xu J, Luo J, Zhao X, Nat. Comm. 2020, 11, 1604.

[9]. Gao W, Zhang Y, Zhang Q, Zhang L, Ann. Biomed. Eng. 2016, 44, 2049. [PubMed: 26951462]

[10]. Park J, Choi JH, Kim S, Jang I, Jeong S, Lee JY, Acta Biomater. 2019, 97, 141. [PubMed: 31352108]

[11]. Phan LM, Vo TA, Hoang TX, Cho S, Nanomaterials 2021, 11, 906. [PubMed: 33918204]

[12]. Paulsen BD, Tybrandt K, Stavrinidou E, Rivnay J, Nat. Mater. 2020, 19, 13. [PubMed: 31427743]

[13]. Balint R, Cassidy NJ, Cartmell SH, Acta Biomater. 2014, 10, 2341. [PubMed: 24556448]

[14]. Tropp J, Rivnay J, J. Mater. Chem. C 2021, 9, 13543.

[15]. Tan P, Wang H, Xiao F, Lu X, Shang W, Deng X, Song H, Xu Z, Cao J, Gan T, Wang B, Zhou X, Nat. Commun. 2022, 13, 358. [PubMed: 35042877]

[16]. Petty AJ, Keate RL, Jiang B, Ameer GA, Rivnay J, Chem. Mater. 2020, 32, 4095.

[17]. a)Bhat MA, Rather RA, Shalla AH, Synth. Met. 2021, 273, 116709;b)Jiang L, Gentile C, Lauto A, Cui C, Song Y, Romeo T, Silva SM, Tang O, Sharma P, Figtree G, Gooding JJ, Mawad D, ACS Appl. Mater. Interfaces 2017, 9, 44124.

[18]. a)Jordan RS, Frye J, Hernandez V, Prado I, Giglio, Abbasizadeh N, Flores-Martinez M, Shirzad K, Xu B, Hill IM, Wang Y, J. Mater. Chem. B 2021, 9, 7258; [PubMed: 34105592] b)Dodda JM, Azar MG, Sadiku R, Macromol. Biosci. 2021, 21, 2100232.

[19]. Kishi R, Hiroki K, Tominaga T, Sano K-I, Okuzaki H, Martinez JG, Otero TF, Osada Y, J. Polym. Sci., Part B: Polym. Phys. 2012, 50, 790.

[20]. van Lith R, Baker E, Ware H, Yang J, Farsheed AC, Sun C, Ameer G, Adv. Mater. Technol. 2016, 1, 1600138.

[21]. Tumbleston JR, Shirvanyants D, Ermoshkin N, Janusziewicz R, Johnson AR, Kelly D, Chen K, Pinschmidt R, Rolland JP, Ermoshkin A, Samulski ET, DeSimone JM, Science 2015, 347, 1349. [PubMed: 25780246]

[22]. a)Peppas NA, Moynihan HJ, Lucht LM, J. Biomed. Mater. Res. 1985, 19, 397; [PubMed: 4055823] b)Wichterle O, Lim D, Nature 1960, 185, 117.

[23]. a)Dursun Usal T, Yucel D, Hasirci V, Int. J. Biol. Macromol. 2019, 121, 699; [PubMed: 30336245] b)Passos MF, Dias DRC, Bastos GNT, Jardini AL, Benatti ACB, Dias CGBT, Maciel Filho, Therm J. Anal. Calorim 2016, 125, 361.

[24]. Beaumont C, Turgeon J, Idir M, Neusser D, Lapointe R, Caron S, Dupont W, D'Astous D, Shamsuddin S, Hamza S, Landry É, Ludwigs S, Leclerc M, Macromolecules 2021, 54, 5464.

[25]. Zhu W, Tringale KR, Woller SA, You S, Johnson S, Shen H, Schimelman J, Whitney M, Steinauer J, Xu W, Yaksh TL, Nguyen QT, Chen S, Mater. Today 2018, 21, 951.

[26]. a)Dai T, Qing X, Zhou H, Shen C, Wang J, Lu Y, Synth. Met. 2010, 160, 791;b)Yang J, Choe G, Yang S, Jo H, Lee JY, Biomater. Res. 2016, 20, 31. [PubMed: 27708859]

[27]. Keate RL, Tropp J, Serna C, Rivnay J, Cell. Mol. Bioeng. 2021, 14, 501. [PubMed: 34777607]

[28]. a)Chen P, Li L, Dong L, Wang S, Huang Z, Qian Y, Wang C, Liu W, Yang L, ACS Biomater. Sci. Eng. 2021, 7, 841; [PubMed: 33715375] b)Camacho P, Behre A, Fainor M, Seims KB, Chow LW, Biomater. Sci. 2021, 9, 6813; [PubMed: 34473149] c)Ansari S, Khorshidi S, Karkhaneh A, Acta Biomater. 2019, 87, 41. [PubMed: 30721785]

[29]. Song S, Amores D, Chen C, McConnell K, Oh B, Poon A, George PM, Sci. Rep. 2019, 9, 19565.

[30]. Wang Y, Wang Q, Luo S, Chen Z, Zheng X, Kankala RK, Chen A, Wang S, Regener. Biomater. 2021, 8, 1.

[31]. Gong HY, Park J, Kim W, Kim J, Lee JY, Koh W-G, ACS Appl. Mater. Interfaces 2019, 11, 47695.

[32]. Kislinger T, Gramolini AO, Pan Y, Rahman K, MacLennan DH, Emili A, Mol. Cell. Proteomics 2005, 4, 887. [PubMed: 15824125]

[33]. Seymour AJ, Shin S, Heilshorn SC, Adv. Healthcare Mater. 2021, 10, 2100644.

[34]. Guo J, Yu Y, Wang H, Zhang H, Zhang X, Zhao Y, Small 2019, 15, 1805162.b)Feig VR, Tran H, Lee M, Liu K, Huang Z, Beker L, Mackanic DG, Bao Z, Adv. Mater. 2019, 31, 1902869.

[35]. Dong Y, Wang S, Ke Y, Ding L, Zeng X, Magdassi S, Long Y, Adv. Mater. Technol. 2020, 5, 2070037.

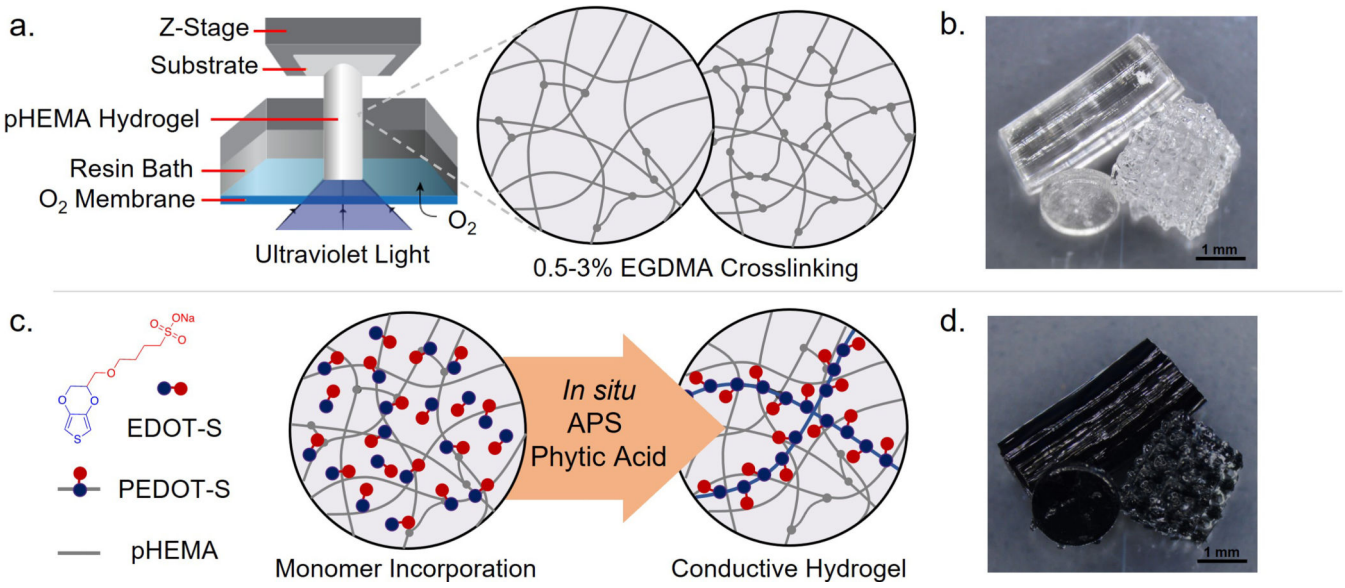

Figure 1.

Functionalization Scheme of μCLIP-printed pHEMA Hydrogels a) pHEMA gels were printed using a μCLIP printer with varying levels of EGDMA in the resin bath to determine the optimal crosslinking level required to obtain structures <100 μm. b) A variety of form factors (discs, rods, and scaffolds) were utilized to systematically evaluate material parameters related to EGDMA. c) After printing, the pHEMA structures were soaked in a solution of EDOT-S and subsequently polymerized to yield PEDOT-S functionalized hydrogels. d) Disc, rod, and scaffold PEDOT-pHEMA structures were all successfully functionalized with PEDOT-S.

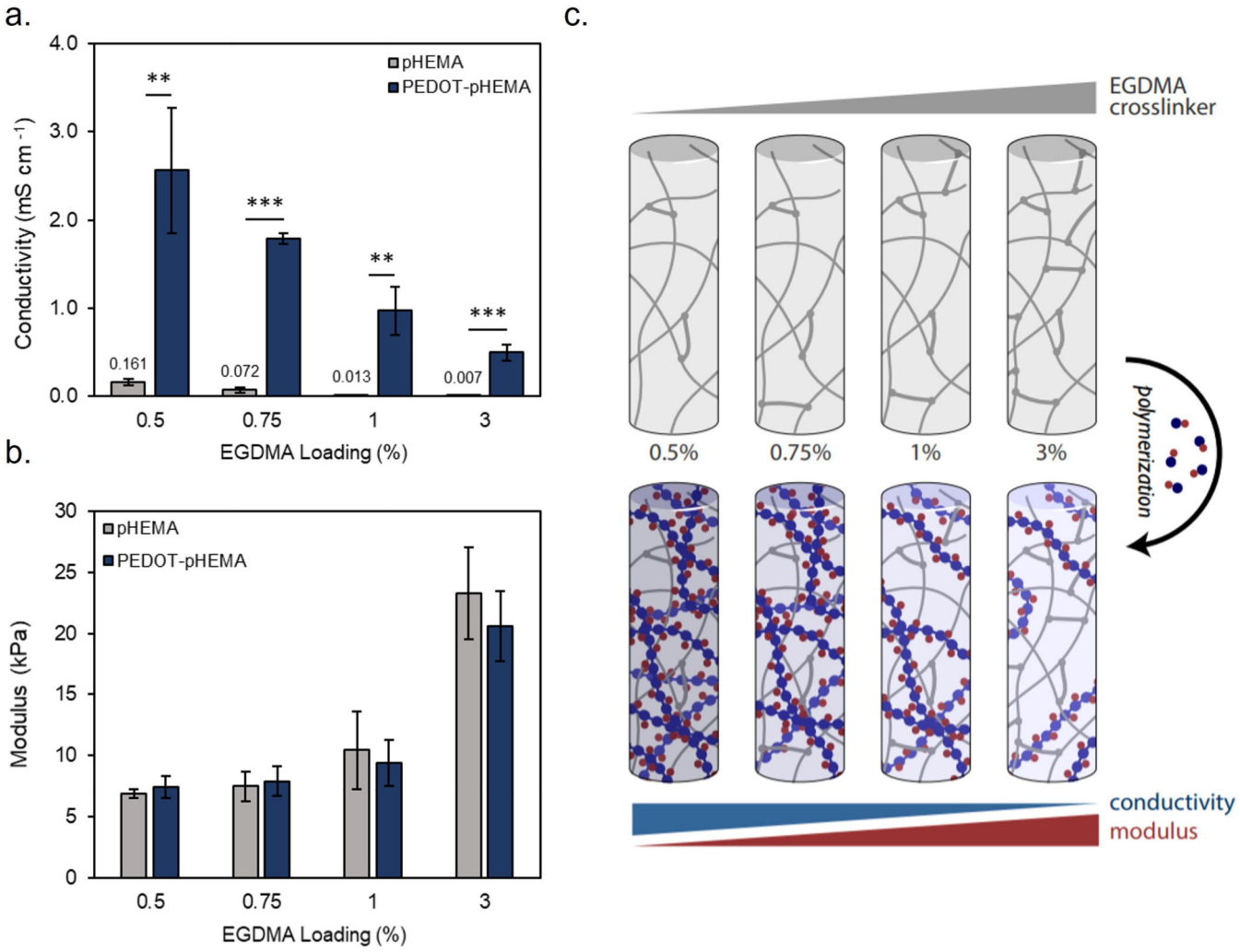

Figure 2.

PEDOT-pHEMA rod characteristics depend on EGDMA crosslinking a) EIS was performed to estimate impedance, and thus conductivity, of PEDOT-pHEMA rods (n = 3). b) Mechanical testing was performed to examine how EGDMA loading influenced pHEMA compressive modulus. The linear portions of the stress-strain curves of rod compression were analyzed to calculate the elastic moduli of the rods (n = 3). c) These trends, taken together, reveal that EGDMA crosslinking increases material stiffness and reduces overall monomer loading into the hydrogel matrix, thus reducing PEDOT-S content and hydrogel conductivity.

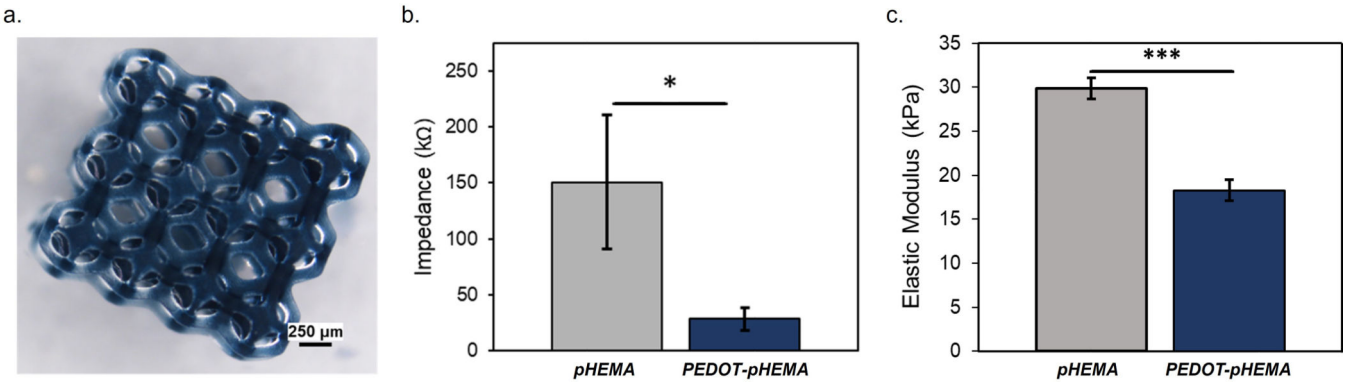

Figure 3.

PEDOT-S Incorporation Improves Scaffold Electroactivity, Decreases Modulus a) Qualitative examination of scaffolds following PEDOT-S incorporation reveals a visible color change verifying the presence of conductive polymer in the hydrogel matrix. b) pHEMA and PEDOT-pHEMA scaffolds were analyzed via EIS to measure changes in scaffold impedance with functionalization (n = 3). c) Compression testing was performed on the scaffolds to determine the influence of PEDOT-S on composite mechanical properties (n = 3).

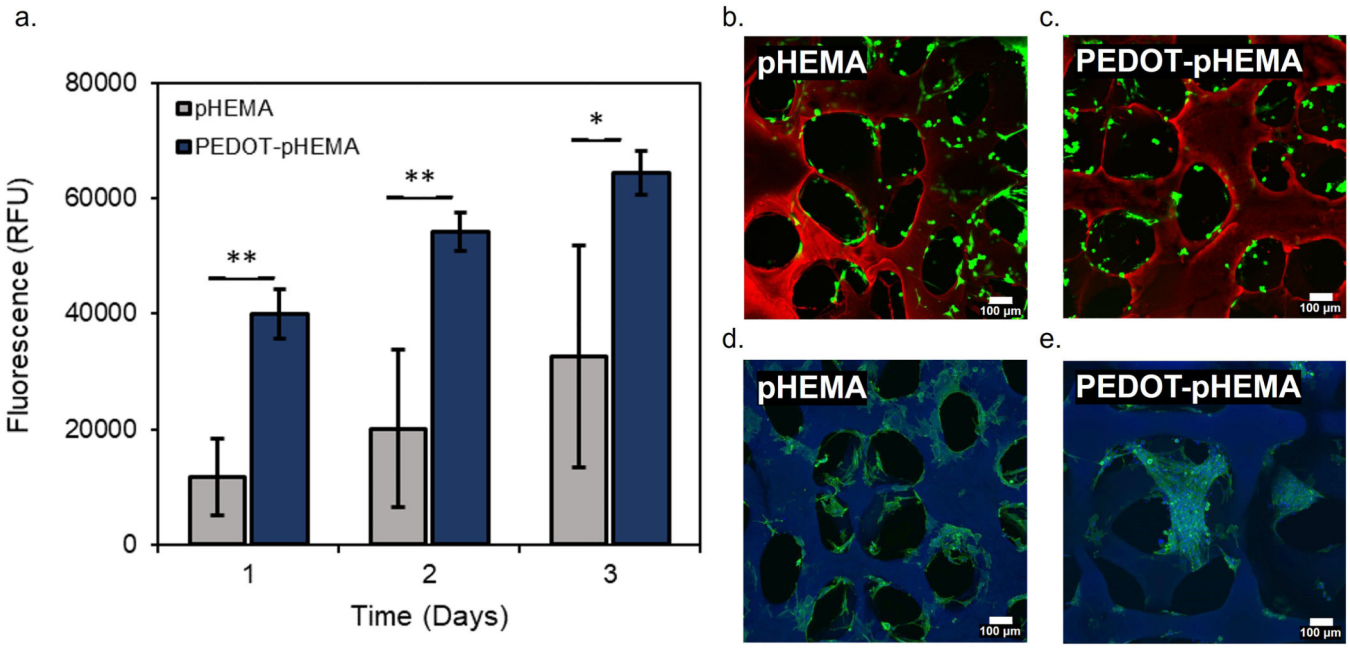

Figure 4.

PEDOT-pHEMA Promote Myoblast Viability a) alamarBlue cell viability was performed to screen PEDOT-pHEMA scaffolds for cytotoxic effects (n = 3). b,c) Live/dead staining was performed to qualitatively examine the distribution of cells on the scaffolds. Living cells are shown in green and dead cells, as well as the scaffold reflectance, are shown in red. d,e) F-actin was stained to observe how pHEMA and PEDOT-pHEMA scaffolds differentially influenced cell morphology. F-actin is shown in green and cell nuclei, as well as the scaffold reflectance, are shown in blue.